

Kent Academic Repository

Full text document (pdf)

Citation for published version

Zanoli, Clément and Kullmer, Ottmar and Kelley, Jay and Bacon, Anne-Marie and Demeter, F and Dumoncel, Jean and Fiorenza, Luca and Grine, Fred E. and Hublin, Jean-Jacques and Tuan, Nguyen and Huong, Nguyen and Pan, Lei and Schillinger, Burkhard and Schrenk, Friedemann and Skinner, Matthew M. and Ji, Xueping and Macchiarelli, Roberto (2019) Evidence for increased

DOI

Link to record in KAR

<https://kar.kent.ac.uk/72814/>

Document Version

Author's Accepted Manuscript

Copyright & reuse

Content in the Kent Academic Repository is made available for research purposes. Unless otherwise stated all content is protected by copyright and in the absence of an open licence (eg Creative Commons), permissions for further reuse of content should be sought from the publisher, author or other copyright holder.

Versions of research

The version in the Kent Academic Repository may differ from the final published version.

Users are advised to check <http://kar.kent.ac.uk> for the status of the paper. **Users should always cite the published version of record.**

Enquiries

For any further enquiries regarding the licence status of this document, please contact:

researchsupport@kent.ac.uk

If you believe this document infringes copyright then please contact the KAR admin team with the take-down information provided at <http://kar.kent.ac.uk/contact.html>

Evidence for increased hominid diversity in the Early-Middle Pleistocene of Java, Indonesia

Clément Zanolli^{1*}, Ottmar Kullmer^{2,3}, Jay Kelley^{4,5,6}, Anne-Marie Bacon⁷, Fabrice Demeter^{8,9}, Jean Dumoncel¹, Luca Fiorenza^{10,11}, Frederick E. Grine¹², Jean-Jacques Hublin¹³, Nguyen Anh Tuan¹⁴, Nguyen Thi Mai Huong¹⁴, Lei Pan^{15,16}, Burkhard Schillinger¹⁷, Friedemann Schrenk^{2,3}, Matthew M. Skinner^{13,18}, Xueping Ji¹⁹ & Roberto Macchiarelli^{20,21}

¹Laboratoire AMIS, UMR 5288 CNRS, Université Toulouse III Paul Sabatier, Toulouse, France.

²Department of Palaeoanthropology, Senckenberg Research Institute and Natural History Museum

Frankfurt, Frankfurt a.M., Germany. ³Department of Paleobiology and Environment, Institute of

Ecology, Evolution, and Diversity, Goethe University Frankfurt, Germany. ⁴Institute of Human

Origins and School of Human Evolution and Social Change, Arizona State University, Tempe,

USA. ⁵Department of Paleobiology, National Museum of Natural History, Smithsonian Institution,

Washington D.C., USA. ⁶Department of Human Evolutionary Biology, Harvard University,

Cambridge, USA. ⁷Laboratoire AMIS UMR5288, Université Paris Descartes, Faculté de

chirurgie dentaire, Montrouge, France. ⁸UMR 7206 CNRS, Muséum National d'Histoire Naturelle,

Paris, France. ⁹Center for GeoGenetics, Copenhagen, Denmark. ¹⁰Department of Anatomy and

Developmental Biology, Monash University, Melbourne, Australia. ¹¹Earth Sciences, University of

New England, Armidale, Australia. ¹²Department of Anthropology and Department of Anatomical

Sciences, Stony Brook University, Stony Brook, USA. ¹³Department of Human Evolution, Max

Planck Institute for Evolutionary Anthropology, Leipzig, Germany. ¹⁴Anthropological and

Palaeoenvironmental Department, The Institute of Archaeology, Hanoi, Vietnam. ¹⁵Key Laboratory

of Vertebrate Evolution and Human Origins, Institute of Vertebrate Paleontology and

Paleoanthropology, Chinese Academy of Sciences, Beijing, China. ¹⁶State Key Laboratory of

Palaeobiology and Stratigraphy, Nanjing Institute of Geology and Palaeontology, Chinese Academy

of Sciences, Nanjing, China ¹⁷Heinz Maier-Leibnitz Center (FRM-II), Technische Universität

München, Garching, Germany. ¹⁸School of Anthropology and Conservation, University of Kent,

Canterbury, UK. ¹⁹Department of Paleanthropology, Yunnan Institute of Cultural Relics and

Archaeology, Kunming 650118, China. ²⁰UMR 7194 CNRS, Muséum National d'Histoire Naturelle,

Paris, France. ²¹Unité de Formation Géosciences, Université de Poitiers, France.

Since the first discovery of *Pithecanthropus (Homo) erectus* by E. Dubois at Trinil in 1891, over 200 hominid dentognathic remains have been collected from the Early-Middle Pleistocene deposits of Java, Indonesia, forming the largest palaeoanthropological collection in Southeast Asia. Most of these fossils are currently attributed to *H. erectus*. However, because of the substantial morphological and metric variation in the Indonesian assemblage, some robust specimens, such as the partial mandibles Sangiran 5 and Sangiran 6a, were formerly variably allocated to other taxa (*Meganthropus palaeojavanicus*, *Pithecanthropus dubius*, *Pongo* sp.). To resolve the taxonomic uncertainty surrounding these and other contentious Indonesian hominid specimens, we used Occlusal Fingerprint Analysis to reconstruct their chewing kinematics, and also used various morphometric approaches based on microtomography to examine internal dental structures. Our results confirm the presence of *Meganthropus* as a Pleistocene Indonesian hominid distinct from *Pongo*, *Gigantopithecus* and *Homo*, and further reveal that Eugene Dubois' *Homo erectus* paratype molars from 1891 are not hominin (human lineage), but

46 **instead are more likely to belong to *Meganthropus*.**

47

48 During the Quaternary, ~~eustatic fluctuations~~ episodes of glacial eustasy combined with tectonic uplift
49 and ~~volcanic events~~ volcaniclastic deposition periodically altered the palaeobiogeography of the
50 Sunda region. These physical and resultant environmental changes facilitated or inhibited intermittent
51 faunal exchanges with the Asian mainland¹ and influenced the evolutionary dynamics of the local
52 faunas, including hominids². The presence of hominids (great apes and humans) in Southeast Asia
53 during the Early and Middle Pleistocene is well documented in the fossil record, with at least three
54 firmly established genera: *Gigantopithecus*, *Pongo* and *Homo*³⁻⁶. The existence of a putative “mystery
55 ape” has also been evoked⁷. Due to the implied vicariance and relict survivorship accompanying these
56 geomorphological events, the appraisal of palaeobiodiversity at a regional scale is difficult. The
57 presence of *Homo* in insular Southeast Asia since the Early Pleistocene has been amply documented
58 by cranial, dental and postcranial remains³. Conversely, besides apart from four isolated teeth recently
59 discovered in Peninsular Malaysia⁸, only a few dental specimens representing *Pongo* sp. have been
60 reported from the Early and Middle Pleistocene deposits of Indonesia⁹. Because of the convergence
61 in molar crown size and overall morphology between fossil *Homo* and *Pongo*, the taxonomic
62 diagnosis of many Asian Early Pleistocene hominid dentognathic specimens has been debated for
63 over a century, especially concerning isolated teeth and occlusally worn specimens^{10,11}. The resulting
64 taxonomic confusion has affected the historical debate on the evolution of the genus *Homo* in
65 Southeast Asia and, more generally, the assessment of Pleistocene hominid palaeobiodiversity⁷.

66 Using three-dimensional virtual imaging, we reassess the taxonomic assignment ~~of~~ of two isolated
67 maxillary molars from Trinil (Trinil 11620 and Trinil 11621)^{10,11}, paratypes of *H. erectus*¹², and of the
68 partial mandibles Sangiran 5, the holotype of *Pithecanthropus dubius*¹³, and Sangiran 6a, the holotype
69 of *Meganthropus paleojavanicus*^{13,14,15}, all currently considered to be *H. erectus*¹⁶⁵⁻¹⁶⁸. We also re-
70 examine the mandibular specimen Arjuna 9, regarded as a robust *H. erectus* similar to Sangiran
71 ~~6a~~¹⁷ 6a¹⁹, and seven isolated upper and lower permanent molar crowns from the Early-Middle
72 Pleistocene Sangiran Dome formations (FS-77, SMF-8855, SMF-8864, SMF-8865, SMF-8879,
73 SMF-8898 and SMF-10055), provisionally labelled as *Pongo* sp., but whose taxonomic identity
74 remains problematic (Figure 1, Supplementary Figure 1 and Supplementary Material). The analyses
75 and/or examined features include Occlusal Fingerprint Analysis, enamel distribution and relative
76 enamel thickness, crown-root surface area proportions, enamel-dentine junction topography, and pulp
77 chamber morphology. We compare the results from this Indonesian assemblage with similar data from
78 extant and fossil *Homo* and *Pongo*, as well as the fossil hominids *Sivapithecus* (Late Miocene, South
79 Asia), *Lufengpithecus* (Late Miocene, southern China), and *Gigantopithecus* (Pleistocene, China and
80 Southeast Asia)²⁰⁺⁸ (Supplementary Tables 1-4).

82 **Results**

83 One important distinction between humans and non-human apes concerns their dietary ecology and
 84 feeding behaviours, reflected in their masticatory apparatus by different morphological adaptations
 85 and structural characteristics^{19,20,21,22}. Occlusal Fingerprint Analysis^{24,3} of crown wear patterns reveals
 86 that all robust Indonesian hominid molars suitable for this investigation (9 of 13) exhibit an ape-like
 87 functional macrowear pattern that differs significantly ($p < 0.05$) from that of extant and extinct
 88 hominin samples, including Javanese *H. erectus* (Figure 2 and Supplementary Table 5). This pattern
 89 is characterised by a high dominance of power stroke Phase II over Phase I, evidenced by enlarged
 90 Phase II wear facets (Supplementary Table 6). In contrast, humans and extinct hominins, including
 91 Chinese and Indonesian *H. erectus*, display proportionately larger buccal Phase I wear facets,
 92 indicative of distinct masticatory behaviour (Figure 2).

93 Patterns of enamel distribution are sensitive indicators of dietary adaptations and taxonomic
 94 affinities in anthropoids²⁰². Morphometric cartographies distinguish between hominin and ape
 95 patterns: in the former, the thickest enamel is deposited on the “functional cusps” rather than on the
 96 “guiding” cusps²²⁰, while in apes, and notably in *Pongo*, it lies at the periphery of the occlusal basin²⁴²⁻
 97 ²⁶⁴. Our analyses reveal that all but one of the modestly worn hominid molars from Java (n=8) show
 98 an ape pattern. The maxillary molar Trinil 11620 displays even relatively thicker ~~peripheral~~ enamel
 99 at the periphery of the occlusal basin than is typically found in *Pongo*, more closely approximating
 100 the Miocene apes *Sivapithecus* and *Lufengpithecus* (Figure 3). Conversely, the specimen SMF-8865
 101 closely resembles the condition characterising African and Indonesian *H. erectus*, showing the
 102 thickest enamel localized on the buccal cusps, while Arjuna 9, FS-77, SMF8855, SMF-8864 and
 103 SMF-8879 have the thickest enamel distributed along the marginal ridges around the occlusal basin.
 104 Crown tissue proportions, including the commonly used Relative Enamel Thickness
 105 index^{22,24,25,24,26,27}, overlap across all extinct and extant samples and do not discriminate the Javanese
 106 robust specimens (Supplementary Figure 2 and Supplementary Tables 7-8).

107 Crown-root surface area proportions have also been demonstrated to show a strong phylogenetic
 108 signal, independent of feeding adaptations in tooth morphology²⁸⁶. Both upper molars from Trinil and
 109 the lower post-canine teeth of Sangiran 6a and Arjuna 9 exhibit proportionally large root surfaces
 110 compared to the lateral (non-occlusal) crown area, resembling pongines and *Lufengpithecus* and
 111 differing substantially from *Homo* (Figure 4, Supplementary Figure 3 and Supplementary Table 419).

112 The topography of the enamel-dentine junction (EDJ), which reliably distinguishes fossil and
 113 extant hominid taxa^{224,2426,2729}, approximates the inner enamel epithelium of the developing tooth and
 114 provides useful information about taxon-specific processes underlying crown growth²⁹⁷. Six of the
 115 Javanese lower molars show a cingulum-like, mesiodistally extended buccal protostylid at the EDJ,

116 which is distinct from the morphology commonly found in *Homo* and *Pongo* but similar to the
117 condition expressed by the Miocene Chinese ape *Lufengpithecus* (Supplementary Figure 4; see also
118 Supplementary Figure 5 for the lower P4P4 EDJ morphology). The specimen SMF-8865 does not
119 show the same coarse wrinkling pattern at the EDJ as the other robust Indonesian hominids, or the
120 dense crenulation pattern typical of *Pongo*, but rather resembles the *H. erectus* condition
121 (Supplementary Figure 4).

122 We also performed geometric morphometric (GM) analyses of the molar EDJ to compare the
123 Indonesian fossil specimens to an assemblage of fossil and extant hominids (Figure 5). The results
124 show statistical discrimination between *Pongo* and *Homo* and unambiguously classify the robust
125 Javanese specimens as non-human apes, again with the exception of SMF-8865 (Supplementary
126 Table 910). Indeed, except for the latter specimen, the EDJ shape of this Javanese sample of robust
127 teeth is distinguished from *Homo* and overlaps those of *Pongo* and *Lufengpithecus*, even if some
128 specimens like the holotype of *Meganthropus*^{13,14,15}, Sangiran 6a, are outside the variation of *Pongo*
129 (Figure 5, Supplementary Figures 86). As in fossil *Pongo*²⁴², *Gigantopithecus*²²⁴, *Sivapithecus* and
130 *Lufengpithecus*, the EDJ of these teeth consistently exhibits a low topography with higher mesial than
131 distal dentine horns. Interestingly, comparable results are obtained when the same analysis is
132 performed on the lower P4P4 of Sangiran 6a (Supplementary Figures 97-108 and Supplementary
133 Table 101). Conversely, in *Homo*^{264,27-29} and in SMF-8865 as well, the EDJ typically shows higher
134 relief, with dentine horns of sub-equal height and more distally-set buccal cusps (Figure 5). In light
135 of this, it is noteworthy that a pongine-like endostructural signature (but different from that typical of
136 *Pongo*) was recently identified in an isolated deciduous mandibular molar from the Early Pleistocene
137 of Sangiran that was originally labelled as *Meganthropus*¹³ *Meganthropus*¹⁴, but later allocated to
138 early *Homo* (rev. in ref. 2426).

139 While the taxonomic significance of the EDJ is supported by previous studies²⁷⁹, that of pulp
140 chamber shape has not been systematically evaluated. However, marked morphological differences
141 are notable in the height, thickness and shape of the pulp chamber between fossil and extant hominid
142 taxa (Supplementary Figures 96-107). Accordingly, we performed a preliminarily GM analysis
143 limited to the four extant hominid genera. Our results demonstrate that *Homo* and *Pongo* are
144 statistically distinguished by pulp chamber morphology (Supplementary Material and Supplementary
145 Figure 11). Based on these results, three-dimensional landmark-based analyses of the shape of the
146 pulp chamber (not possible for SMF-8865) were thus extended to the fossil specimens. Similar to the
147 analyses of the EDJ, they clearly discriminate the robust Javanese specimens from *Homo*
148 (Supplementary Table 910). However, in contrast to the results of EDJ shape, the shape of the pulp
149 chamber also distinguishes most of the fossil specimens forming the Javanese assemblage from
150 *Pongo* (except for SMF-8879) and ~~shows overlap with~~ approximates *Lufengpithecus* (Figure 5 and

151 Supplementary Figure 12).

152 When only non-hominin taxa are considered in the GM analyses of the EDJ and pulp chamber, the
153 robust Indonesian molars are generally distinguished from *Pongo* (except for SMF-8879, which falls
154 close to or within the *Pongo* range of variation) and approximate the Miocene representatives,
155 especially *Lufengpithecus* (Figure 6 and Supplementary Figures 13-14).

156

157 Discussion

158 Based on multiple ~~independent~~ aspects of dental morphology, our re-analysis of this long-
159 controversial sample of robust Pleistocene dentognathic specimens from Java demonstrates that, with
160 the exception of the isolated crown SMF-8865, which we attribute to *H. erectus*, all the specimens
161 investigated here most likely represent non-hominin species. Moreover, Trinil 11620, Trinil 11621,
162 Sangiran 5, Sangiran 6a, Arjuna 9, FS-77 and SMF-8864 are dentally distinct from *Pongo* and
163 represent a third ape lineage in addition to *Pongo* and *Gigantopithecus* that survived beyond the
164 Miocene in South-eastern Asia. We propose to allocate this material to the resurrected species
165 *Meganthropus palaeojavanicus* von Koenigswald, 1950^{14,153,14}, but as a non-hominin. The holotype
166 is Sangiran 6a and the other specimens are paratypes. Consequently, *Pithecanthropus dubius*¹⁵³
167 becomes a junior synonym of *Meganthropus palaeojavanicus*.

168 Unlike most apes, Sangiran 6a and Sangiran 9¹⁴⁻¹⁷ lack the canine/P3 honing complex and the P3
169 is non-sectorial, being more similar to the P4 with reduced crown height, a relatively prominent
170 metaconid (thus being clearly bicuspid) and a more buccolingually oriented crown major axis. In all
171 these features, *Meganthropus* is similar to Plio-Pleistocene hominins, which might argue for
172 *Meganthropus* being a hominin rather than a non-hominin hominid as we conclude from our analysis
173 of internal dental structure. However, there are other fossil apes in which the P3 is non-sectorial and
174 converges on a hominin-like morphology, most strikingly among megadont species that have
175 undergone marked canine reduction such the Late Miocene *Indopithecus*³⁰, and especially the
176 Pleistocene *Gigantopithecus*^{6,31}, in which the P3 is typically bicuspid. A relatively low-crowned and
177 more transversely oriented P3 associated with some degree of canine reduction (at least with respect
178 to its cervical dimensions) also characterizes the Late Miocene megadont *Ouranopithecus*³². While
179 having a sectorial P3, *Lufengpithecus* also shows strong expression of the metaconid, in some cases
180 bordering on a bicuspid morphology³³.

181 Concerning Trinil 11620, this tooth was among those in another recent attempt to sort out the
182 identities of Pleistocene dental remains, mostly from China but including several teeth from Southeast
183 Asia as well¹¹. Other than 2D enamel thickness and EDJ topography, that study examined different
184 aspects of dental morphology than those examined here, and, with the exception of Trinil 11620, on
185 an entirely different sample. While Trinil 11620 is identified *a priori* as a hominin in a previous

186 study¹¹, it is based on a prior analysis³⁴ to decide only whether it should be assigned to *Homo* or
187 *Pongo* without considering the possible presence of an additional Pleistocene ape lineage in Southeast
188 Asia in addition to *Pongo* and *Gigantopithecus*, no results or conclusions are reported for it other than
189 a long-period developmental line periodicity of either 6 or 7. These values are well below the reported
190 range of periodicities for fossil or extant *Pongo* and a value of 6 would be an unusually low value for
191 fossil or extant *Homo*^{11,34,35}. Although we did not examine long-period line periodicity and there is
192 substantial variation in long-period line periodicities in hominid taxa^{34,35}, the low value for Trinil
193 11620 could perhaps be considered as additional support for the assignment of this tooth to
194 *Meganthropus*.

195 In keeping with its prior definition, *Meganthropus* is distinguished from *Homo* by having
196 absolutely large teeth^{143,4415}, a mandibular corpus with a thick and rounded inferior border, a large
197 extramolar sulcus and strong lateral prominence¹⁴⁺¹⁶¹⁵⁻¹⁷, molarised premolars, and low molar crowns
198 with coarse wrinkling converging toward the centre of the occlusal ~~surface~~¹³ surface^{14,4415}. Our results
199 demonstrate that *Meganthropus* is further distinguished from *Homo* by an ape-like molar occlusal
200 macrowear pattern, peripherally-distributed thicker molar enamel, low crowned EDJ with relatively
201 short dentine horns, a particularly slender pulp shape with high horns, and lower crown/root surface
202 area proportions. It further differs from penecontemporaneous *H. erectus* by the presence of a
203 cingulum-like protostylid in both the enamel and the underlying EDJ. This feature is commonly found
204 in *Australopithecus* and *Paranthropus*, but *Meganthropus* differs from these two hominins by its ape-
205 like occlusal wear pattern (Supplementary Figure 15), thicker peripheral enamel (whereas thicker
206 enamel is found at the cusp tip in australopiths³⁶²⁸), the lower EDJ topography, and more slender pulp
207 chamber with vertically elongated pulp horns (Supplementary Figure ~~15~~¹⁶). As a further consequence
208 of recognizing *Meganthropus* as non-hominin, certain features commonly regarded as characteristic
209 of hominins, such as the loss of the canine/P3 honing complex, lack of a marked mandibular simian
210 shelf, moderately mesiodistally elongated premolars with a double root and premolar/molar size
211 proportions^{124,1314+1617}, more likely represent homoplastic traits in *Meganthropus*. From our results, it
212 is also evident that, aside from marked differences in mandibular morphology and proportions,
213 *Meganthropus* differs from *Pongo* by having laterally-positioned molar dentine horns, a slender pulp
214 chamber, and a cingulum-like expression of the protostylid (Figure 6 and Supplementary Figures 4
215 and ~~6~~⁹). *Meganthropus* is also clearly distinct from *Gigantopithecus*, the latter displaying higher-
216 crowned and narrower molars with low bulbous cusps and rounded crests, a large cuspule formed by
217 a lobe between the protoconid and metaconid giving the lower molars a distinctive cusp pattern
218 comprised of two pairs of main cusps arranged peripherally, a line of smaller midline cusps that
219 includes the talonid cuspule and the hypoconulid, the lack or faint expression of the protostylid, strong
220 buccolingual mid-crown waisting⁶, thicker occlusal enamel, and higher EDJ topography²²⁴ (for a

221 [detailed differential diagnosis of *Meganthropus*, see Supplementary Material section 3 and Table 12\).](#)

222 We provisionally assign SMF-8879 to *Pongo* sp. Future analyses should clarify the taxonomic
223 status of the specimens SMF-8855, SMF-8898 and SMF-10055, currently regarded as pongines, but
224 which also share some features with the Asian Miocene apes, as well as other specimens from Early
225 Pleistocene Java whose status continues to be debated (e.g., Sangiran 8, Sangiran 9, Sangiran
226 27)^{165,1617}.

~~Evidence concerning palaeoenvironments is compatible with the above conclusions regarding
227 hominid palaeobiodiversity. During the Quaternary, episodes of glacial eustasy, tectonic uplift, and
228 volcanioclastic deposition structured the dispersal routes of hominids and other fauna, and exerted a
229 strong influence on the habitats of Southeast Asia². The Early Pleistocene palaeoenvironments of
230 Sangiran and Trinil in which the hominids lived likely included a variety of mixed and temporally
231 shifting habitats. These included large areas of open woodland, indicated by the presence of *Stegodon*
232 *trigonocephalus*, an abundance of large bovids (e.g., *Bubalus palaeokerabau*, *Bibos*
233 *palaeosondaicus*), and various cervids and carnivores (e.g., *Panthera*)^{2,29}, and by a pollen record
234 revealing the dominance of sedges, grasses, and ferns, with scattered trees such as *Acacia*, leaf-flower
235 and Indian albizia³⁰. Freshwater marsh and lake-edge habitats, as well as wet grasslands with scattered
236 shrubs, were also found in lower elevations of the landscape, indicated by a variety of aquatic and
237 semi-aquatic vertebrate (*Hexaprotodon*, tortoise, crocodiles, turtles, fish) and invertebrate species^{2,29}.
238 The occurrence of two monkey species, *Macaca fascicularis* and *Trachypithecus cristatus*, is a strong
239 indicator for the presence of forested areas in the ecosystem as well².~~

~~The mosaic nature of habitats at Sangiran and Trinil has recently been corroborated by stable
241 isotope analysis³¹. Tooth enamel $\delta^{13}\text{C}$ and $\delta^{18}\text{O}$ values indicate that some bovids (*Bubalus*
242 *palaeokerabau*, *Duboisia santeng*) and cervids (*Axis lydekkeri*) were preferentially grazers, with a
243 strongly C_4 -dominated diet in an open woodland, while suids (*Sus brachygnathus*) express either a
244 C_3 - or C_4 -signal, indicating that closed-canopy C_3 -vegetation was also present in the area³¹. The tiger
245 *Panthera tigris* consumed prey with a C_3 - C_4 -mixed diet³¹. In such a dynamic and complex mosaic
246 environment, it is therefore not surprising that multiple hominid lineages would have inhabited
247 Southeast Asia at this time.~~

249 Across most of Eurasia, apes became extinct prior to the end of the Miocene. They survived into
250 the Plio-Pleistocene only in South-eastern Asia, represented by *Gigantopithecus* and *Pongo*, both
251 known from southern-most China into Southeast Asia^{5,3237}. To these can now be added *Meganthropus*
252 from Java, formerly suggested to be an ape by some^{142,143,144,15} but only confidently demonstrated to
253 be so by the comparative analyses presented here. [As demonstrated by paleobotanical, paleontological
254 and geochemical proxies^{2,38-40}, the Early to Middle Pleistocene palaeoenvironments of Sangiran and
255 Trinil included a variety of mixed and temporally shifting habitats, ranging from open woodland areas](#)

256 to dense forests capable of supporting the presence of multiple large-bodied hominid species in
257 addition to at least two arboreal monkeys, *Macaca fascicularis* and *Trachypithecus cristatus*². Of the
258 ~~Miocene~~ apes present during the late Miocene in South and Southeast Asia, *Sivapithecus*,
259 *Khoratpithecus*, and *Lufengpithecus*, *Meganthropus* appears to be dentally most closely related to the
260 last, evidenced by the presence in both of low-cusped and wrinkled molar crowns^{21+9,33+1.42} with a
261 squat EDJ, an extended protostylid and a slender pulp chamber (Figure 5, Supplementary Figures 4
262 and 69). In contrast, *Sivapithecus* and *Khoratpithecus* have higher, more bunodont molars with
263 marked mid-crown buccolingual constriction^{19,20+1.22} and proportionally higher dentine horns in
264 *Sivapithecus* ~~has proportionally higher dentine horns~~-(Figure 5).
265

266 **Conclusions**

267 During the Early-Middle Pleistocene, at least three and perhaps four hominid genera inhabited what
268 is now Indonesia: *Homo*, *Pongo* and *Meganthropus*, with the possible presence of
269 ~~*Gigantopithecus*³²~~*Gigantopithecus*³⁷. This is a higher level of diversity than previously recognised
270 and is particularly noteworthy for the late survival of two to three large ape lineages. Whether related
271 to the expansion of *H. erectus*, palaeoenvironmental changes, competition with *Pongo* or
272 *Gigantopithecus*, or some combination of these factors, *Meganthropus* did not persist beyond the
273 Middle Pleistocene, leaving only three species of the genus *Pongo* (*P. pygmaeus*, *P. abelii* and *P.*
274 *tapanuliensis*) subsisting today in remote and protected Indonesian ~~localities~~³⁴localities⁴³.
275

276 **Methods**

277 **X-ray and neutron microtomography.** Except for the Trinil molars and Sangiran 5 (see below), all
278 Javanese hominid specimens studied here (Sangiran 6a, Arjuna 9, FS-77, SMF-8855, SMF-8864,
279 SMF-8865, SMF-8879, SMF-8898 and SMF-10055) were scanned using the X-ray microfocus
280 sources (X- μ CT) at: the Helmholtz-Zentrum Berlin (equipment CONRAD II instrument), the
281 Department of Human Evolution of the Max Plank Institute of Leipzig (equipment BIR ACTIS
282 225/300), the University of Poitiers (equipment X8050-16 Viscom AG), and the Seckenberg
283 Research Institute (Phoenix Nanotom s 180). Acquisitions were performed according to the
284 following parameters: 100-160 kV, 0.11-90 μ A, 0.14-0.36° of angular step. The final volumes were
285 reconstructed with voxel sizes ranging from 20.8 to 40.7 μ m. The two Trinil molars (11620 and
286 11621) were scanned by SR- μ CT ~~at the~~on beamline ID 19 of the European Synchrotron Radiation
287 Facility ~~at~~of Grenoble using absorption mode with an isotropic voxel size of 31.12 μ m³ at an energy
288 of 60 keV¹⁰. The dataset of 632 images is available in 8 bits .tif format at the ESRF Paleontological
289 Database (<http://paleo.esrf.eu>). The X- μ CT acquisitions of the comparative fossil and extant

290 hominid specimens were performed using various equipments with the following parameters: 95-
291 145 kV, 0.04-0.40 μ A, 0.17-0.36° of angular step. The final volumes were reconstructed with voxel
292 sizes ranging from 8.3 to 60.0 μ m.

293 The specimens Sangiran 5 and Sangiran 6a were scanned by neutron microtomography (n-
294 μ CT)^{35-39,44-48} at the ANTARES Imaging facility (SR4a beamline) of the Heinz Maier-Leibnitz
295 Center (FRM II) of Technische Universität München. The neutron beam originated from the cold
296 source of the FRM II reactor, with an energy range mostly from 3 to 20 meV, a collimation ratio of
297 L/D=500 (ratio between sample-detector distance and collimator aperture) and an intensity of $6.4 \times$
298 10^7 n/cm²s. A 20 μ m Gadox screen was used to detect neutrons. Both a cooled scientific CCD
299 camera (Andor ikon-L) and cooled scientific CMOS camera (Andor NEO) were used as detectors.
300 The final virtual volume of these specimens was reconstructed with an isotropic voxel size of 20.45
301 μ m.

302
303 **Data processing.** Some specimens showed low contrasts between the enamel and dentine in some
304 parts of the dataset, precluding automatic segmentation. In such cases, enamel and dentine were
305 segmented using the magic wand tool in Avizo 8.0 (FEI Visualization Sciences Group) and manual
306 corrections were locally applied. ~~The Use of the interpolation tool was limitedly used in the to~~ areas
307 where the distinction between enamel and dentine ~~could not be precisely demarcated was not~~
308 ~~accurately distinguishable~~. A volumetric reconstruction was then generated for each specimen. In
309 most cases, the contrast resolution enabled carrying out a semi-automatic threshold-based
310 segmentation following the half-maximum height method (HMH⁴⁰⁹) and the region of interest
311 thresholding protocol (ROI-Tb⁵⁰⁴¹) taking repeated measurements on different slices of the virtual
312 stack⁵¹⁴². Because the detection of the tissue interfaces is based on attenuation at the boundary of a
313 structure in both X-ray and neutron-based microtomography, we performed a threshold-based
314 segmentation with manual corrections, as usually applied for X-ray acquisitions^{52,53,43,44}. We
315 quantified the degree of morphological and dimensional coherence between the X-ray
316 microtomography (X- μ CT) and n- μ CT datasets of Sangiran 6a. The superimposed EDJ based on
317 the X- μ CT and n- μ CT records show maximum 240 μ m differences and an average of 65.7 μ m
318 variation (Supplementary Figure ~~16~~17). Considering the difference in voxel size of the two original
319 datasets (39.33 μ m and 20.45 μ m for the X-ray and neutron data, respectively), the differences in
320 LM1 enamel volume (349.26 μ m³ and 346.61 μ m³), dentine-pulp volume (529.1 μ m³ and
321 526.7 μ m³) and crown volume (878.4 μ m³ and 873.3 μ m³) are ~~inferior to~~ less than 1% and can be
322 regarded as negligible.

323
324 **Occlusal Fingerprint Analyses.** The analysis of dental wear facets enables the reconstruction of

occlusal ~~behaviour~~²¹behaviour²³. Qualitative wear facet analysis performed by Mills⁴⁵-Mills⁵⁴ already led to the conclusion that in primates and insectivores the occlusal power stroke of the chewing cycle consists of two phases (buccal Phase and lingual Phase), which ~~are~~were later determined as Phase I and Phase II^{46,47,55,56}. The chewing cycle starts with the preparatory (closing) stroke where three-body contact (tooth-food-tooth) leads to puncture-crushing activity with rare contacts of antagonistic crowns. Real chewing starts with ~~the~~Phase I^{47,56}, ~~whereas-in which~~ during stereotypic cycles tooth-tooth contacts may occur more commonly, producing guiding buccal and lingual Phase I facets through shearing activity along the buccal slopes of the buccal and lingual cusps of the lowers and complementary facets on the lingual cusp slopes of the upper molars. Phase I ends in maximum intercuspatation (centric occlusion) leading into Phase II with a more or less lateral shift of the lower jaw leading to grinding activity until the last antagonistic contacts. During the recovery stroke the jaws open with no dental contacts^{23,23,25,47,56}. The Phase I and Phase II pathway of the power stroke is recorded in the wear facet pattern on the ~~occlusal-occluding~~ molars^{23,48-54,57-60}. To assess the occlusal motion pattern(s) characteristic of the Early Pleistocene robust Javanese hominid ~~dental-assembly~~teeth considered ~~in this~~here, we applied Occlusal Fingerprint Analysis (OFA) to attribute proportions of wear facet areas to power stroke phases in order to compare occlusal motion patterns in a sample of extant and fossil Asian great apes and *Homo*. Occlusal macrowear areas, including wear facets ~~after~~following Maier and Schneck⁴⁸Schneck⁵⁷, were identified on virtual surface models of upper and lower molar crowns following the OFA method described in Kullmer et al.²³ and Fiorenza et al.^{61,52}. The 3D surface data acquisition derived either from μ CT datasets or from 3D surface scanning ~~such as~~with a smartSCAN-HE (Breuckmann GmbH). Scans ~~have been~~were taken either from originals or from high resolution casts ~~providing that provide~~ reasonable resolution of macrowear for mapping wear facet ~~areas~~⁴⁹areas⁵⁸. We used the modular software package PolyWorks® 2016 (InnovMetric Inc.) to edit the surface models. The polyline tool in the software module IMEdit was applied to interactively mark and fit closed polylines onto the models ~~surfaces~~ along the perimeter of wear facets in each tooth crown. By re-triangulation of the crown surfaces, the polylines became integrated into the surface models. ~~For To~~measuring each wear facet area, triangles were selected up to each polyline curve, grouped and color-coded following the occlusal compass^{23,50,59}. The area measurement tool in IMEdit was used to compute area in mm² for each wear facet. Wear facet areas were ~~summarized~~summed for chewing cycle power stroke phases^{47,53,56,62}. Buccal Phase 1 (BPh I), lingual Phase 1 (LPh I) and Phase 2 (Ph II) facet area data were grouped for comparing percentage distribution of wear. ~~In respect of comparing~~To compare power stroke movements only, flat worn areas on cusp tips, identified as tip crushing ~~areas~~⁵²areas⁶¹, were excluded ~~from measuring~~ because this type of tissue loss usually results from puncture-crushing activity^{56,62,47,53} and is not attributable

360 with certainty to one of the two power stroke phases. Percentage results are illustrated in ternary
361 plots. Each corner of the triangle represents 100% of one variable. Accordingly, a sample with an
362 equal distribution of wear facet areas will be placed in the center of the triangle. The plots were
363 generated using the ggtern package v.2.2.~~2~~⁵⁴-~~2~~⁶³ in R v.3.4~~64~~⁵⁵. The R package RVAideMemoire 0.9-
364 ~~66~~⁶⁵~~56~~ was used to perform one-way permutational multivariate analysis of variance
365 (PERMANOVA) on the three variables (BPh I, LPh I and Ph II) ~~distinctly~~separately for the
366 maxillary and mandibular molar samples. A Bray-Curtis similarity matrix was calculated based on a
367 9999 permutations parameter. For both upper and lower molars the test was significant ($p < 0.05$),
368 with values for the pseudo-F model of 18.78 and 13.98 and R^2 coefficients of 0.53 and 0.57,
369 respectively. Post-hoc PERMANOVA pairwise comparisons were run with a false discovery rate
370 (FDR) correction (Supplementary Table 5).

371

372 **3D tooth tissue proportions.** Premolar and molar crowns and roots were digitally isolated at the
373 cervix along the best-fit plane and surface rendering was performed using unconstrained smoothing
374 for visualization, while constrained smoothing was applied for the quantitative analyses. For the
375 molar teeth, seven linear, surface, and volumetric variables describing tooth tissue proportions were
376 digitally measured or calculated on the molars: V_e , the volume of the enamel cap (mm^3); V_{cdp} ; the
377 volume of the crown dentine+pulp (mm^3); V_c , the total crown volume; SEDJ, the surface area of
378 the enamel-dentine junction (mm^2); V_{cdp}/V_c , the percent of the crown volume that is dentine and
379 pulp (%); 3D AET ($=V_e/\text{SEDJ}$), the three-dimensional average enamel thickness (mm); 3D RET
380 ($=3\text{D AET}/V_{cdp}^{1/3} * 100$), the scale-free three-dimensional relative enamel thickness (see
381 methodological details in ~~the refs.~~ 242,2836,6657). For both premolars and molars, the following
382 parameters were also calculated: LEA, the lateral enamel surface area (mm^2)⁶⁷~~58~~; RA, the total root
383 surface area (mm^2)⁵⁸; CRR ($=\text{LEA}/\text{RA} * 100$), the crown-root ratio (%) (see Figure 4,
384 Supplementary Figures 2-3 and Supplementary Tables 3,4,7,8). Because of ~~its~~the advanced degree
385 of occlusal wear in Sangiran 6a~~degree~~, only crown-root proportions were assessed for the
386 mandibular fourth premolar ~~of Sangiran 6a~~.

387 Intra- and interobserver accuracy tests ~~for accuracy~~ of the measures run by two observers
388 provided differences $< 5\%$. Adjusted Z-score analyses^{68,69}~~59,60~~ were performed on three tooth crown
389 tissue proportions parameters (V_{cdp}/V_c , 3D AET and 3D RET) for the robust Indonesian hominid
390 maxillary (Trinil 11620, Trinil 11621 and SMF-8898) and mandibular molars (Arjuna 9, FS-77,
391 SMF-8855, SMF-8864, SMF-8865, SMF-8879 and SMF-10055) and were compared with ~~some~~
392 extant and fossil hominid samples (Supplementary Figure 17-18 and Supplementary Table 8). This
393 statistical test was also applied for the CRR parameter on the maxillary molars Trinil 11620 and
394 Trinil 11621, on the mandibular fourth premolar of Sangiran 6a and on the molars of Sangiran 6a

395 and Arjuna 9 preserving complete roots (Figure 4, Supplementary Figure 3 and Supplementary
396 Table 119). This statistical method allows the comparison of unbalanced samples, which is often the
397 case when dealing with the fossil record, using the Student's t inverse distribution following the
398 formula: $[(x-m)/(s*\sqrt{1+1/n})]/(\text{Student.t.inverse}(0.05;n-1))$, where x is the value of the variable
399 (e.g., $V_{\text{edp}}/V_{\text{e}}$ of Arjuna 9 M2); m is the mean of the same variable for a comparative sample (e.g.,
400 $V_{\text{edp}}/V_{\text{e}}$ of MH); n is the size of the comparative sample (e.g., 41 individuals); and s is the
401 standard deviation of the comparative sample (e.g., sd: 3.93).
402

403 **Enamel thickness distribution cartographies.** The 3D topographic mapping of the site-specific
404 enamel thickness variation was ~~realized~~ generated from the segmented enamel and crown dentine
405 components of unworn to only slightly worn teeth and rendered using chromatic scales⁷⁰⁻⁷⁴~~61-65~~. A
406 rainbow chromatic scale was also used to illustrate gradual variation of enamel thickness, ranging
407 from the thickest (in red) to the thinnest (in blue) (Figure 3).
408

409 **Geometric morphometric analyses.** 3D geometric morphometric (GM) analyses were conducted
410 on the virtual surfaces of the EDJ of the maxillary molars and mandibular fourth premolar and
411 molars. The landmarks were set along the marginal outline of the EDJ occlusal ~~basin~~⁶⁵ basin⁷⁴. For
412 the maxillary molars, six landmarks were set: three at the apex of the paracone, protocone and
413 metacone dentine horns, and three at each intermediate lowest point between two horns along the
414 dentine marginal ridges and oblique crest. For the lower fourth premolar, eight landmarks were ~~put~~
415 placed on the EDJ surface: four at the apex of the protoconid, metaconid, entoconid and hypoconid
416 dentine horns and four at each intermediate lowest point between two horns along the dentine
417 marginal ridge. For the mandibular molars, seven landmarks were placed: four at the apex of the
418 protoconid, metaconid, entoconid and hypoconid dentine horns and three at each intermediate
419 lowest point between two horns along the dentine marginal ridge (located by translating the cervical
420 plane occlusally), except between the two distal horns (because of the variable presence of the
421 hypoconulid, notably in modern humans, this ~~latter~~-cusp and the distal marginal ridge were not
422 considered). While the specimen Trinil 11620 is virtually unworn, the protocone dentine horn apex
423 of Trinil 11621 is affected by wear. It was thus reconstructed based on the intact height and
424 morphology of the paracone, as well as on those of the mesial dentine horns of Trinil 11620. A
425 similar procedure was applied to reconstruct the buccal dentine horns of Sangiran 5 and Sangiran 6a
426 (Figure 1). We also conducted GM analyses on ~~the~~ pulp chamber shape, setting similarly located
427 landmarks on the cavity roof of the maxillary and mandibular molars, but not on that of the lower
428 premolar because of a lack of expression of the distal cusps on its pulp chamber. We performed
429 generalized Procrustes analyses, principal component analyses (PCA) and between-group principal

430 component analyses (bgPCA) based on the Procrustes shape ~~coordinates~~⁶⁶ coordinates⁷⁵ and using
431 genera as groups (Figures 5-6 and Supplementary 8-10 and 12-14). The robust Indonesian hominid
432 specimens were included a posteriori in the bgPCA. The analyses were performed using the
433 package ade4 v.1.7-6~~67~~-6⁷⁶ for R v.3.4⁶⁴⁵⁵. Allometry was tested using multiple regressions⁷⁷⁶⁸ in
434 which the explanatory ~~explanative~~-variable is the centroid size and the dependent variables are the
435 PC and bgPC scores. In all PCA and bgPCA, the first components only show a weak allometric
436 signal ($0.00 < R^2 < 0.30$), the differences between specimens thus mostly representing shape-variation.
437 In order to statistically assess the taxonomic affinities of the robust Indonesian hominid molars, we
438 used a supervised classification method by Support Vector Machine (SVM). Compared with linear
439 discriminant analyses (LDA) and quadratic discriminant analyses (QDA), SVM makes no
440 assumptions about the data, meaning it is a very flexible and powerful method⁷⁸⁶⁹. SVM tests were
441 performed on the PC scores from each GM analysis on the first number of PCs representing needed
442 to achieve more than 95% of the total variability (i.e., 6 to 11 ~~first~~ PCs) (Supplementary Tables 5
443 and ~~10~~11). Leave-2-out cross-validations were run in order to validate the model (predictive
444 accuracy) of classification for the groups including hominins (*Homo*) on the one hand and apes
445 (Ponginae-*Lufengpithecus*) on the other ~~hand~~. ~~Then, we~~ We then tested the attribution of the
446 Indonesian fossil hominid specimens included in the GM analyses (Arjuna 9, Sangiran 5, Sangiran
447 6a, FS-77, SMF-8855, SMF-8864, SMF-8865, SMF-8879, SMF-8898, SMF-10055, Trinil 11620,
448 Trinil 11621) with respect to the model.

449

450 **Data availability.** The authors declare that all data supporting the findings of this study are
451 available within the paper [and its ~~supplementary~~ Supplementary information files].

452

453 **References**

- 454 1. Voris, H.K. Maps of Pleistocene sea levels in Southeast Asia: shorelines, river systems and time
455 durations. *J. Biogeogr.* **27**, 1153-1167 (2000).
- 456 2. Larick, R. & Ciochon, R.L. Early hominin biogeography in island Southeast Asia. *Evol.*
457 *Anthropol.* **24**, 185-213 (2015).
- 458 3. Antón, S.C., Spoor, F., Fellmann, C.D. & Swisher III, C.C. in *Handbook of Paleoanthropology*
459 (eds Henke, W. & Tattersall, I.) 1655-1695 (Springer, New York, 2007).
- 460 4. Ciochon, R.L. in *Out of Africa I: The first hominin colonization of Eurasia* (eds Fleagle, J.G.,
461 Shea, J.J., Grine, F.E., Baden, A.L. & Leakey, R.E.) 111-126 (Springer, Dordrecht, 2010).
- 462 5. Harrison, T., Jin, C., Zhang, Y., Wang, Y. & Zhu, M. Fossil *Pongo* from the Early Pleistocene
463 *Gigantopithecus* fauna of Chongzuo, Guangxi, southern China. *Quat. Intl.* **354**, 59-67 (2014).
- 464 6. Zhang, Y. & Harrison, T. *Gigantopithecus blacki*: a giant ape from the Pleistocene of Asia
465 revisited. *Am. J. Phys. Anthropol.* **162**, 153-177 (2017).
- 466 7. Ciochon, R.L. The mystery ape of Pleistocene Asia. *Nature* **459**, 910-911 (2009).
- 467 8. Ibrahim, Y.K. *et al.* First discovery of Pleistocene orangutan (*Pongo* sp.) fossils in Peninsular
468 Malaysia: Biogeographic and paleoenvironmental implications. *J. Hum. Evol.* **65**, 770-797
469 (2013).

- 470 9. Kaifu, Y., Aziz, F. & Baba, H. New evidence of the existence of *Pongo* in the Early/Middle
471 Pleistocene of Java. *Geol. Res. Dev. Centre Bandung* **27**, 55-60 (2001).
- 472 10. Smith, T.M. *et al.* Taxonomic assessment of the Trinil molars using non-destructive 3D
473 structural and development analysis. *PaleoAnthropol.* **2009**, 117-129 (2009).
- 474 ~~10-11.~~ 11. Smith, T.M. *et al.* [Disentangling isolated dental remains of Asian Pleistocene hominins and](https://doi.org/10.1371/journal.pone.0204737)
475 [pongines. *PLoS One* **13**, e0204737 <https://doi.org/10.1371/journal.pone.0204737> \(2018\).](https://doi.org/10.1371/journal.pone.0204737)
- 476 ~~11-12.~~ 12. Dubois, E. *Pithecanthropus erectus, eine menschenaehnliche Ubergangsform aus Java.*
477 *Landesdruckerei, Batavia* (1894).
- 478 ~~12-13.~~ 13. Tyler, D.E. Sangiran 5, ("*Pithecanthropus dubius*"), *Homo erectus*, "*Meganthropus*", or
479 *Pongo*? *Hum. Evol.* **18**, 229-242 (2003).
- 480 ~~13-14.~~ 14. Dubois, E. *Pithecanthropus erectus, eine menschenaehnliche Ubergangsform aus Java.*
481 *Landesdruckerei, Batavia* (1894).
- 482 ~~14-15.~~ 15. von Koenigswald, G.H.R. Fossil hominids of the Lower Pleistocene of Java: Trinil. *18th*
483 *Intl. Geol. Congr.* **9**, 59-61 (1950).
- 484 ~~15-16.~~ 16. Weidenreich, F. Giant early man from Java and South China. *Anthropol. Pap. Am. Mus. Nat.*
485 *Hist.* **40**, 1-134 (1945).
- 486 ~~16-17.~~ 17. Kaifu, Y. *et al.* Taxonomic affinities and evolutionary history of the Early Pleistocene
487 Hominids of Java: Dentognathic evidence. *Am. J. Phys. Anthropol.* **128**, 709-726 (2005).
- 488 18. Kaifu, Y., Aziz, F. & Baba, H. Hominin mandibular remains from Sangiran: 1952-1986
489 collection. *Am. J. Phys. Anthropol.* **128**, 497-519 (2005).
- 490 ~~17-19.~~ 19. Schwartz, J.H. & Tattersall, I. Defining the genus *Homo*. *Science* **349**, 931-932 (2015).
- 491 ~~18-20.~~ 20. Grimaud-Hervé, D. & Widiyanto, H. in *Origine des Peuplements et Chronologie des Cultures*
492 *Paléolithiques dans le Sud-Est Asiatique.* (eds Sémah, F., Falguères, C., Grimaud-Hervé, D. &
493 Sémah, A.M.) 331-358 (Artcom', Paris, 2001).
- 494 ~~19-21.~~ 21. Begun, D.R. *A Companion to Paleoanthropology.* Wiley-Blackwell, Chichester (2013).
- 495 ~~20-22.~~ 22. Fleagle, J.G., *Primate Adaptation and Evolution, 3rd Edition.* Elsevier, London (2013).
- 496 ~~21-23.~~ 23. Teaford, M.F. & Ungar, P.S. in *Handbook of Palaeoanthropology, 2nd Edition* (eds Henke,
497 W. & Tattersall, I.) 1465-1494. (Springer, New York, 2015).
- 498 ~~22-24.~~ 24. Kullmer, O., *et al.* Occlusal Fingerprint Analysis (OFA) - quantification of tooth wear
499 pattern. *Am. J. Phys. Anthropol.* **139**, 600-605 (2009).
- 500 ~~23-25.~~ 25. Olejniczak, A.J., *et al.* Molar enamel thickness and dentine horn height in *Gigantopithecus*
501 *blacki*. *Am. J. Phys. Anthropol.* **135**, 85-91 (2008).
- 502 ~~24-26.~~ 26. Fiorenza, L., Nguyen, N.H. & Benazzi, S. Stress distribution and molar macrowear in *Pongo*
503 *pygmaeus*: A new approach through Finite Element and Occlusal Fingerprint Analyses. *Hum.*
504 *Evol.* **30**, 215-226 (2015).
- 505 ~~25-27.~~ 27. Zanolli, C. *et al.* The Early Pleistocene deciduous hominid molar FS-72 from the Sangiran
506 Dome of Java, Indonesia: A taxonomic reappraisal based on its comparative endostructural
507 characterization. *Am. J. Phys. Anthropol.* **157**, 666-674 (2015).
- 508 ~~26-28.~~ 28. Smith, T.M. *et al.* Variation in enamel thickness within the genus *Homo*. *J. Hum. Evol.* **62**,
509 395-411 (2012).
- 510 ~~27-29.~~ 29. Kupczik, K., Olejniczak, A.J., Skinner, M.M. & Hublin, J.J. Molar crown and root size
511 relationship in anthropoid primates. *Front. Oral Biol.* **13**, 16-22 (2009).
- 512 30. Skinner, M.M. *et al.* Dental trait expression at the enamel-dentine junction of lower molars in
513 extant and fossil hominoids. *J. Hum. Evol.* **54**, 173-186 (2008).
- 514 31. Simons, E. L. & Chopra, S. R. K. *Gigantopithecus* (Pongidae, Hominoidea) a new species
515 [from North India. *Postilla* **138**, 1-18 \(1969\).](https://doi.org/10.1007/BF02692111)
- 516 ~~32.~~ 32. Wang, W. New discoveries of *Gigantopithecus blacki* teeth from Chuifeng Cave in the Buning
517 Basin, Guangxi, south China. *J. Hum. Evol.* **57**, 229-240 (2009).
- 518 ~~33.~~ 33. Koufos, G.D. & de Bonis, L. New material of *Ouranopithecus macedoniensis* from late
519 [Miocene of Macedonia \(Greece\) and study of its dental attrition. *Geobios* **39**, 223-243 \(2006\).](https://doi.org/10.1016/j.geobios.2006.03.001)
- 520 ~~34.~~ 34. Xu, Q. & Lu, Q. *Lufengpithecus lufengensis – An Early Member of Hominidae.* Science Press,
521 [Beijing](https://doi.org/10.1007/978-7-03-014111-1) (2007).

- 522 [35. Smith, T.M., et al. Dental ontogeny in Pliocene and Early Pleistocene hominins. *PLoS One* **10**,](#)
523 [e0118118 doi:10.1371/journal.pone.0118118 \(2015\).](#)
- 524 [28-36. Smith, T.M. Dental development in living and fossil orangutans. *J. Hum. Evol.* **94**, 92-105](#)
525 [\(2016\).](#)
- 526 [29-37. Olejniczak, A.J., et al. Three-dimensional molar enamel distribution and thickness in](#)
527 [Australopithecus and Paranthropus. *Biol. Lett.* **4**, 406-410 \(2008\).](#)
- 528 [30-38. Bettis III, E.A., et al. Way out of Africa: Early Pleistocene paleoenvironments inhabited by](#)
529 [Homo erectus in Sangiran, Java. *J. Hum. Evol.* **56**, 11-24 \(2009\).](#)
- 530 [31-39. Sémah, A.M., Sémah, F., Djubiantono, T. & Basseur, B. Landscapes and hominids'](#)
531 [environments: Changes between the Lower and the early Middle Pleistocene in Java](#)
532 [\(Indonesia\). *Quat. Intl.* **223-224**, 451-454 \(2010\).](#)
- 533 [32-40. Janssen R., et al. Tooth enamel stable isotopes of Holocene and Pleistocene fossil fauna](#)
534 [reveal glacial and interglacial paleoenvironments of hominins in Indonesia. *Quat. Sci. Rev.* **144**,](#)
535 [145-154 \(2016\).](#)
- 536 [33-41. Noerwidi, S., Siswanto & Widiyanto, H. Giant primate of Java: A new *Gigantopithecus*](#)
537 [specimen from Semedo. *Berkala Arkeologi* **36**, 141-160 \(2016\).](#)
- 538 [42. Kelley, J. & Gao, F. Juvenile hominoid cranium from the late Miocene of southern China and](#)
539 [hominoid diversity in Asia. *Proc. Natl. Acad. Sci. USA.* **109**, 6882–6885 \(2012\).](#)
- 540 [34-43. XuePing, J., et al. Juvenile hominoid cranium from the terminal Miocene of Yunnan, China.](#)
541 [Chin. Sci. Bull. **58**, 3771-3779 \(2013\).](#)
- 542 [35-44. Nater, A. et al. Morphometric, behavioral, and genomic evidence for a new orangutan](#)
543 [species. *Curr. Biol.* **27**, 1-12 \(2017\).](#)
- 544 [36-45. Kardjilov, N., et al. New features in cold neutron radiography and tomography. Part II:](#)
545 [applied energy-selective neutron radiography and tomography. *Nucl. Instr. Meth. Phys. Res. A*](#)
546 [501, 536-546 \(2003\).](#)
- 547 [37-46. Tremsin, A.S., et al. High resolution neutron imaging capabilities at BOA beamline at Paul](#)
548 [Scherrer Institut. *Nucl. Instr. Meth. Phys. Res. A* **784**, 486-493 \(2015\).](#)
- 549 [38-47. Winkler, B. Applications of neutron radiography and neutron tomography. *Rev. Min.*](#)
550 [Geochem. **63**, 459-471 \(2006\).](#)
- 551 [39-48. Schwarz, D., Vontobel, P., Lehmann, E.H., Meyer, C.A. & Bongartz, G. Neutron](#)
552 [tomography of internal structures of vertebrate remains: a comparison with X-ray computed](#)
553 [tomography. *Palaeontol. Electronica* **8** \[http://palaeo-\]\(http://palaeo-electronica.org/2005_2/neutron/issue2_05.htm\)](#)
554 [electronica.org/2005_2/neutron/issue2_05.htm \(2005\).](#)
- 555 [40-49. Sutton, M.D. Tomographic techniques for the study of exceptionally preserved fossils. *Proc.*](#)
556 [R. Soc. B **275**, 1587-1593 \(2008\).](#)
- 557 [41-50. Spoor, C.F., Zonneveld, F.W. & Macho, G.A. Linear measurements of cortical bone and](#)
558 [dental enamel by computed tomography: applications and problems. *Am. J. Phys. Anthropol.*](#)
559 [91, 469-484 \(1993\).](#)
- 560 [42-51. Fajardo, R.J., Ryan, T.M. & Kappelman, J. Assessing the accuracy of high-resolution X-ray](#)
561 [computed tomography of primate trabecular bone by comparisons with histological sections.](#)
562 [Am. J. Phys. Anthropol. **118**, 1-10 \(2002\).](#)
- 563 [43-52. Coleman, M.N. & Colbert, M.W. CT thresholding protocols for taking measurements on](#)
564 [three-dimensional models. *Am. J. Phys. Anthropol.* **133**, 723-725 \(2007\).](#)
- 565 [44-53. Beaudet, A., et al. Neutron microtomography-based virtual extraction and analysis of a](#)
566 [cercopithecoid partial cranium \(STS 1039\) embedded in a breccia fragment from Sterkfontein](#)
567 [Member 4 \(South Africa\). *Am. J. Phys. Anthropol.* **159**, 737-745 \(2016\).](#)
- 568 [45-54. Zanolli, C., et al. Exploring hominin and non-hominin primate dental fossil remains with](#)
569 [neutron microtomography. *Physics Procedia* **88**, 109-115 \(2017\).](#)
- 570 [46-55. Mills, J.R.E. Ideal dental occlusion in the primates. *Dental Practitioner* **6**, 47-63 \(1955\).](#)
- 571 [47-56. Hiiemae, K.M. & Kay, R.F. in *Craniofacial Biology of Primates, 4th International Congress*](#)
572 [of Primatology, Vol. 3 \(eds Montagna, W. & Zingesser, M.R.\), 28-64 \(Karger, Beaverton, 1973\)](#)
- 573 [48-57. Kay, R.F. & Hiiemae, K.M. Jaw movement and tooth use in recent and fossil primates. *Am.*](#)

574 *J. Phys. Anthropol.* **40**, 227-256 (1974).

575 ~~49-58.~~ Maier, W. & Schneck, G. Konstruktionsmorphologische Untersuchungen am Gebiß der
576 hominoiden Primaten. *Zeitschrift für Morphologie und Anthropologie* **72**, 127-169 (1981).

577 ~~50-59.~~ Ulhaas, L., Kullmer, O. & Schrenk, F. In: *Dental Perspectives on Human Evolution: State of*
578 *the Art Research in Dental Paleoanthropology* (eds Bailey, S.E. & Hublin, J.J.) 369-390.
579 (Springer, Dordrecht, 2007).

580 ~~51-60.~~ Kullmer, O., Schulz, D. & Benazzi, S. An experimental approach to evaluate the
581 correspondence between wear facet position and occlusal movements. *Anat. Rec.* **295**, 846-852
582 (2012).

583 ~~52-61.~~ von Koenigswald, W., Anders, U., Engels, S., Schultz, J.A. & Kullmer, O. Jaw movement in
584 fossil mammals: analysis, description and visualization. *Paläontologische Zeitschrift* **87**, 141-
585 159 (2013).

586 ~~53-62.~~ Fiorenza, L., *et al.* Molar macrowear reveals Neanderthal ecogeographic dietary variation.
587 *PLoS One* **6**, e14769 <http://dx.doi.org/10.1371/journal.pone.0014769> (2011).

588 ~~54-63.~~ Janis, C.M. in *Evolutionary Paleobiology of Behavior and Coevolution* (ed Boucot, A.J.)
589 241-259 (Elsevier Science, Amsterdam, 1990).

590 ~~55-64.~~ Hamilton, N. ggtern: An extension to 'ggplot2', for the creation of ternary diagrams. R
591 package version 2.2.2. <https://CRAN.R-project.org/package=ggtern> (2017).

592 ~~56-65.~~ R Development Core Team. *R: A language and environment for statistical computing.*
593 <http://www.R-project.org>. (2017).

594 ~~57-66.~~ Hervé, M. RVAideMemoire: Diverse Basic Statistical and Graphical Functions. R package
595 version 0.9-66. <https://CRAN.R-project.org/package=RVAideMemoire> (2017).

596 ~~58-67.~~ Olejniczak, A.J. *et al.* Dental tissue proportions and enamel thickness in Neanderthal and
597 modern human molars. *J. Hum. Evol.* **55**, 12-23 (2008).

598 ~~59-68.~~ Kupczik, K., & Dean, M.C. Comparative observations on the tooth root morphology of
599 *Gigantopithecus blacki*. *J. Hum. Evol.* **54**, 196-204 (2008).

600 ~~60-69.~~ Maureille, B., Rougier, H., Houët, F. & Vandermeersch, B. Les dents inférieures du
601 néandertalien Regourdou 1 (site de Regourdou, commune de Montignac, Dordogne): analyses
602 métriques et comparatives. *Paleo* **13**, 183-200 (2001).

603 ~~61-70.~~ Scolan, H., Santos, F., Tillier, A.M., Maureille, B. & Quintard, A. Des nouveaux vestiges
604 néanderthaliens à Las Pélénos (Monsempron-Libos, Lot-et-Garonne, France). *Bull. Mém. Soc.*
605 *Anthropol. Paris* **24**, 69-95 (2012).

606 ~~62-71.~~ Macchiarelli, R., Bondioli, L. & Mazurier, A. in: *Technique and Application in Dental*
607 *Anthropology* (eds Irish, J.D. & Nelson, G.C.) 426-448 (Cambridge University Press,
608 Cambridge, 2008).

609 ~~63-72.~~ Macchiarelli, R., Bayle, P., Bondioli, L., Mazurier, A. & Zanolli, C. in *Anthropological*
610 *Perspectives on Tooth Morphology. Genetics, Evolution, Variation* (eds Scott, G.R., Irish, J.D.)
611 250-277 (Cambridge University Press, Cambridge, 2013).

612 ~~64-73.~~ Bayle, P., *et al.* In: *Pleistocene Databases. Acquisition, Storing, Sharing* (eds Macchiarelli,
613 R. & Weniger, G.C.) 29-46 (Wissenschaftliche Schriften des Neanderthal Museums 4,
614 Mettmann, 2011).

615 ~~65-74.~~ Zanolli, C., Bayle, P. & Macchiarelli, R. Tissue proportions and enamel thickness
616 distribution in the early Middle Pleistocene human deciduous molars from Tighenif (Ternifine),
617 Algeria. *C.R. Palevol* **9**, 341-348 (2010).

618 ~~66-75.~~ Zanolli, C. Molar crown inner structural organization in Javanese *Homo erectus*. *Am. J.*
619 *Phys. Anthropol.* **156**, 148-157 (2015).

620 ~~67-76.~~ Mitteroecker, P. & Bookstein, F.L. Linear discrimination, ordination, and the visualization of
621 selection gradients in modern morphometrics. *Evol. Biol.* **38**, 100-114 (2011).

622 ~~68-77.~~ Dray, S. & Dufour, A.B. The ade4 package: implementing the duality diagram for ecologists.
623 *J. Stat. Softw.* **22**, 1-20 (2007).

624 ~~69-78.~~ Bookstein, F.L. *Morphometric Tools for Landmark Data: Geometry and Biology*
625 (Cambridge University Press, Cambridge, 1991).

626 ~~70-79.~~ Gokcen, I. & Peng, J. Comparing Linear Discriminant Analysis and Support Vector
627 Machines. In: *Advances in Information Systems: Second International Conference, ADVIS 2002*
628 (eds Yakhno, T.) 104-113 (Springer-Verlag, Berlin, 2002).
629

630 **Acknowledgements**

631 We thank the Pusat Penelitian Arkeologi of Jakarta and the Balai Pelestarian Situs Manusia Purba
632 of Sangiran, Java, and the French MNHN. We thank the many curators and colleagues who granted
633 access to fossil and recent hominid materials for scanning. We are grateful to D. Grimaud-Hervé, C.
634 Hertler, F. Sémah and H. Widiyanto for support. We thank J. Braga for sharing the
635 microtomographic scans of South African fossil specimens. For scientific discussion, we thank P.
636 Bayle, S. Benazzi, L. Bondioli, J. Braga, M.C. Dean, F. Détroit, [Y. Hou](#), L. Mancini, B. Maureille,
637 A. Mazurier, L. Puymeraul, L. Rook, C. Tuniz, B. Wood. [We would like to express our gratitude to](#)
638 [C. Hemm, L. Hauser, M. Janocha, L. Strzelczyk for their help with the surface scanning and OFA](#)
639 [analysis](#). Scanning of the Vietnamese specimens was funded by the PICS-CNRS to AMB. Research
640 supported by the French CNRS.
641

642 **Author Contributions**

643 The study was initiated by C.Z. during his PhD research project under the supervision of R.M.
644 Microtomographic-based data were collected and elaborated by C.Z., A.M.B., F.D., J.K., O.K.,
645 A.T.N., K.T.N., B.S., J.-J.H., M.M.S., J.X. and R.M. Quantitative data were compiled and analysed
646 by C.Z., J.D., O.K., L.P., M.M.S and R.M. ~~C.Z.,~~ [R.M., O.K. and J.K.](#) wrote the manuscript with
647 contributions from all other authors.
648

649 **Competing interests**

650 The authors declare no competing interests.
651

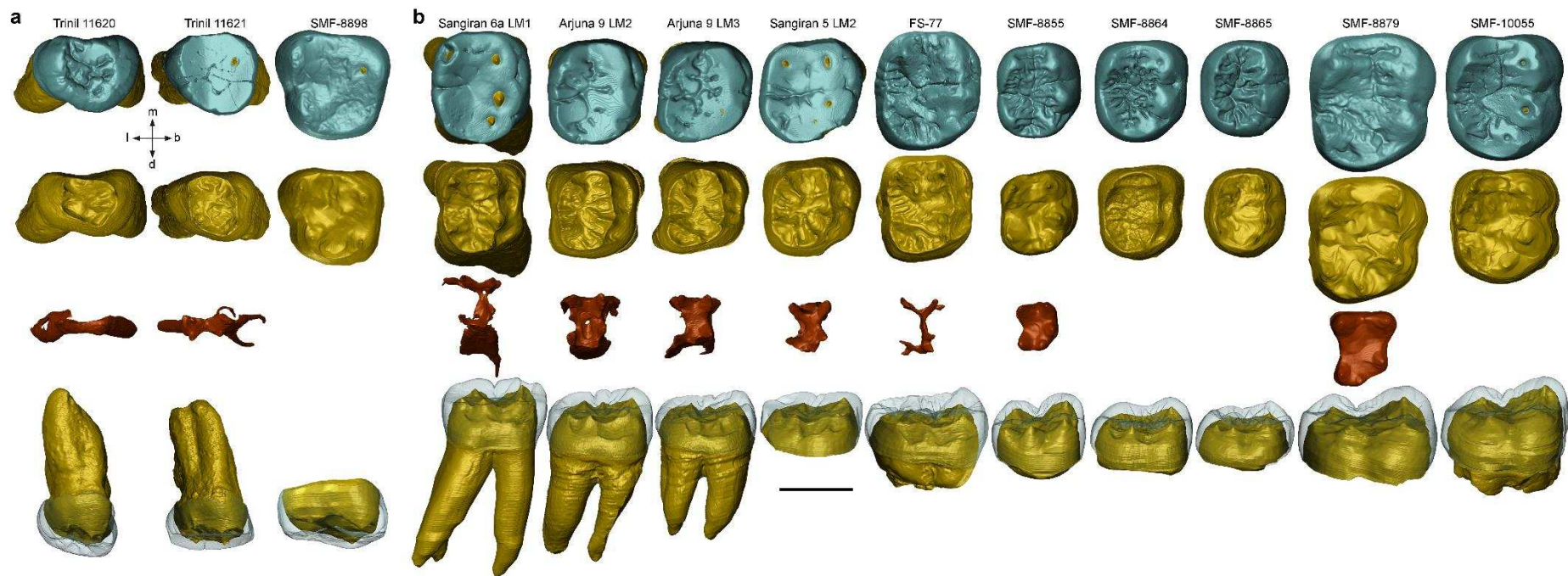
652 **Additional Information**

653 **Supplementary [Information information](#)** is available in the online version of the paper.

654 **Reprints and permissions information** is available at www.nature.com/reprints.

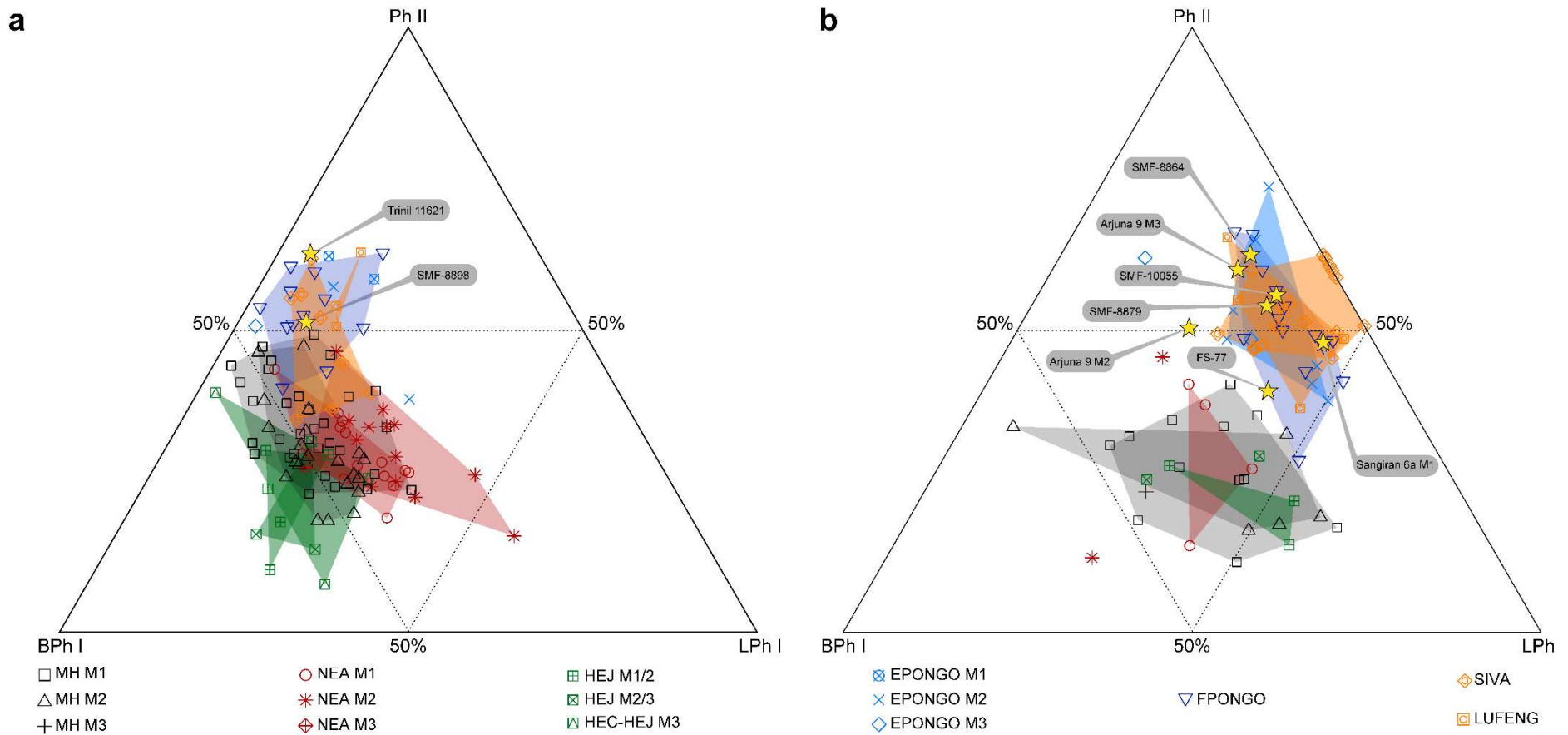
655 **Correspondence and requests for materials** should be addressed to C.Z.

656 (clement.zanolli@gmail.com).
657



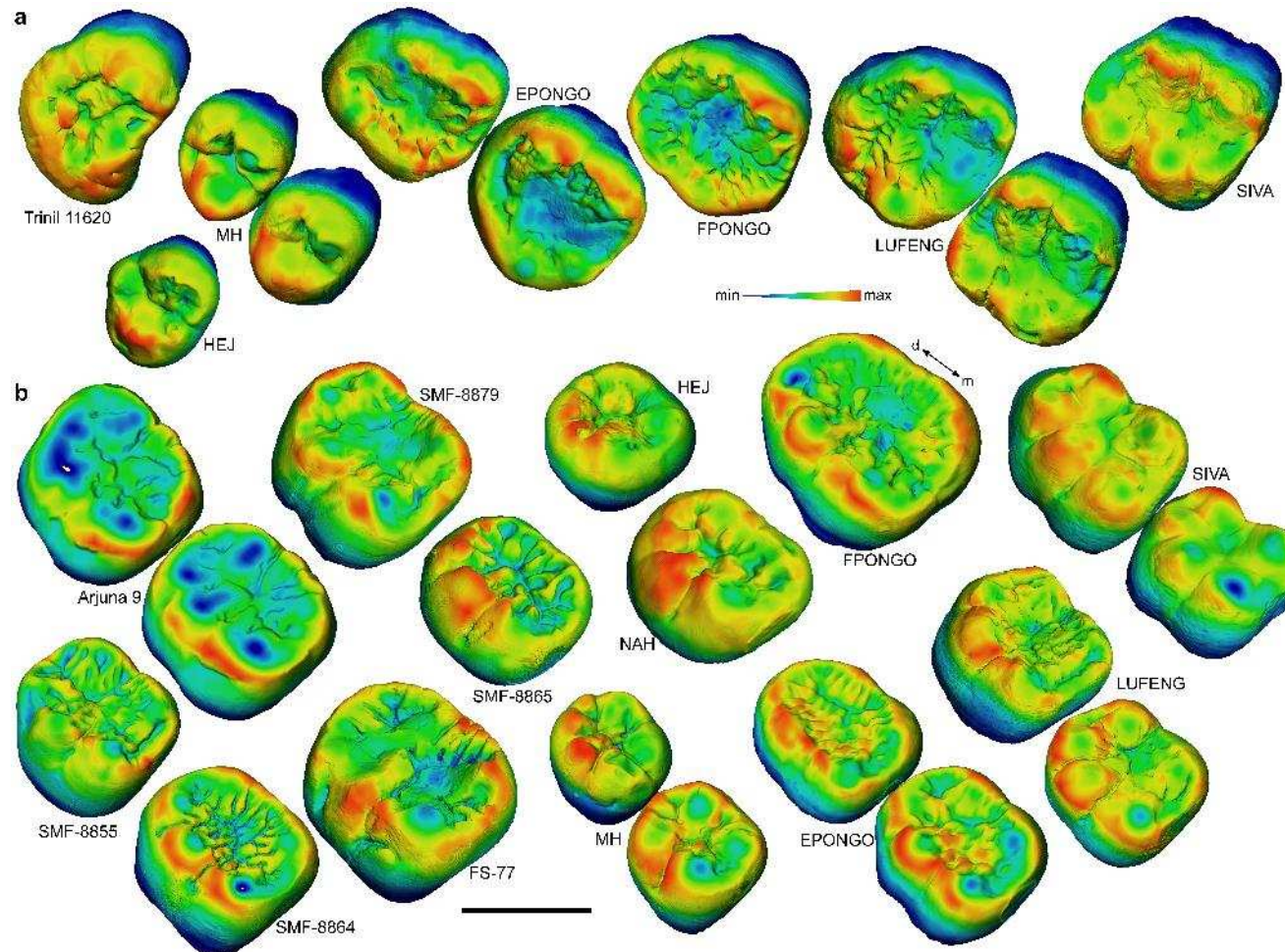
658
 659
 660
 661
 662
 663
 664
 665
 666

Figure 1 | Virtual rendering of the Indonesian hominid teeth examined for taxonomic reassessment. **a**, Maxillary molars. **b**, Mandibular molars (Supplementary Table 1). From the top, the rows show: the external occlusal morphology, the occlusal dentine, the occlusal pulp cavity and the buccal view EDJ with the overlain semi-transparent enamel cap in buccal view. In the bottom row, the EDJ is visible through the enamel imaged in semi-transparency. For SMF-8879, only the crown is imaged. For Trinil 11621, Sangiran 5 and 6a, the worn dentine horn apices were reconstructed following the morphology of the other well-preserved cusps (see Methods). b, buccal; d, distal; l, lingual; m, mesial. Scale bar, 10 mm.



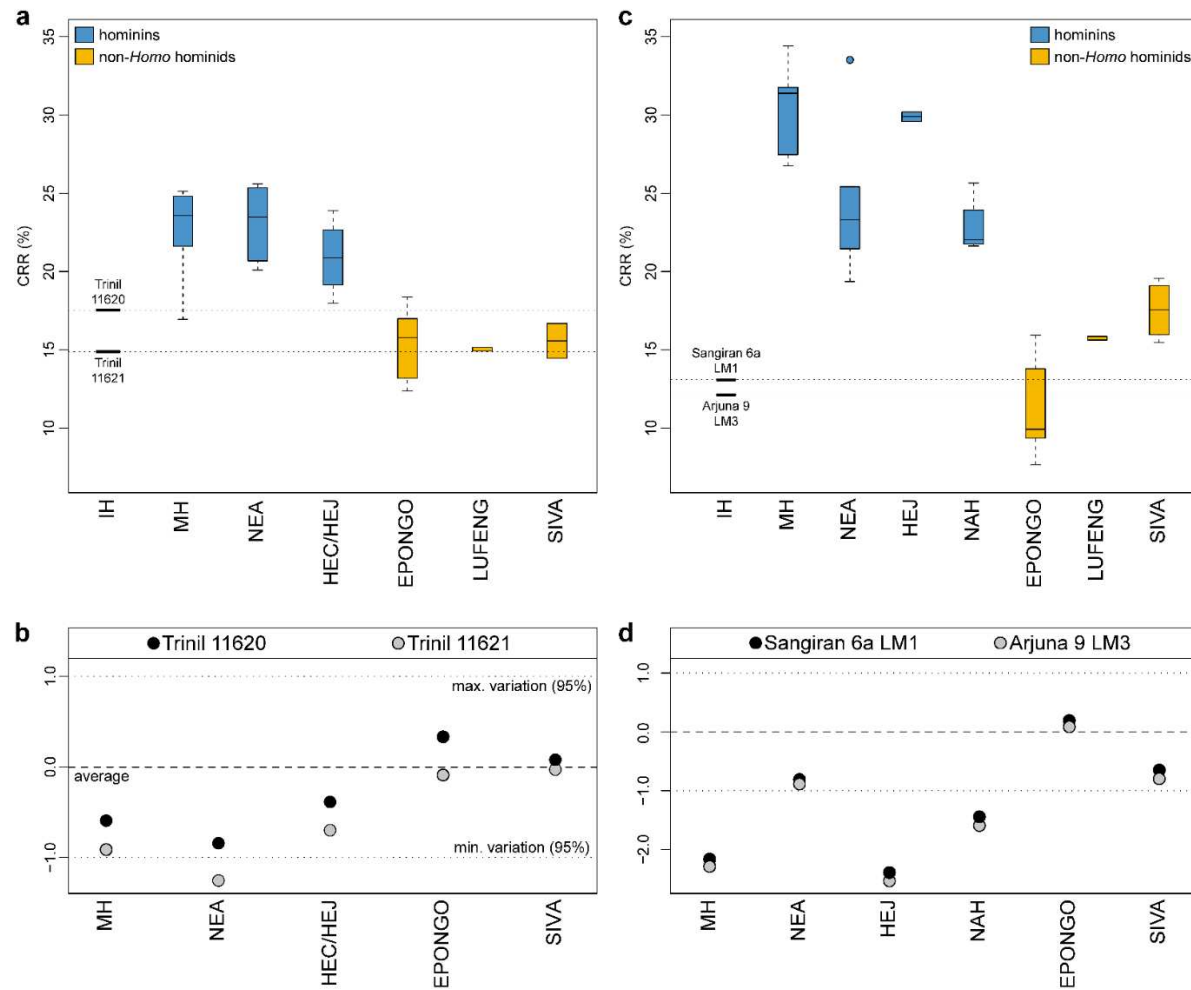
667
668
669
670
671
672
673
674
675

Figure 2 | Occlusal Fingerprint Analyses. **a, b**, Ternary diagram showing the proportions (in %) of relative wear areas of buccal phase I (BPh I), lingual phase I (LPh I), and phase II (Ph II) facets for the Indonesian fossil hominid maxillary (**a**) and mandibular (**b**) molars examined for taxonomic reassessment (Supplementary Table 1) compared with fossil and extant hominid specimens/samples. Each base of the triangle represents a ratio of 0% while the vertices correspond to a percentage of 100%. EPONGO, extant *Pongo*; FPONGO, fossil *Pongo*; HEC, *H. erectus* from China; HEJ, *H. erectus* from Java; LUFENG, *Lufengpithecus*; MH, modern humans; NEA, Neanderthals; SIVA, *Sivapithecus* (Supplementary Table 2).



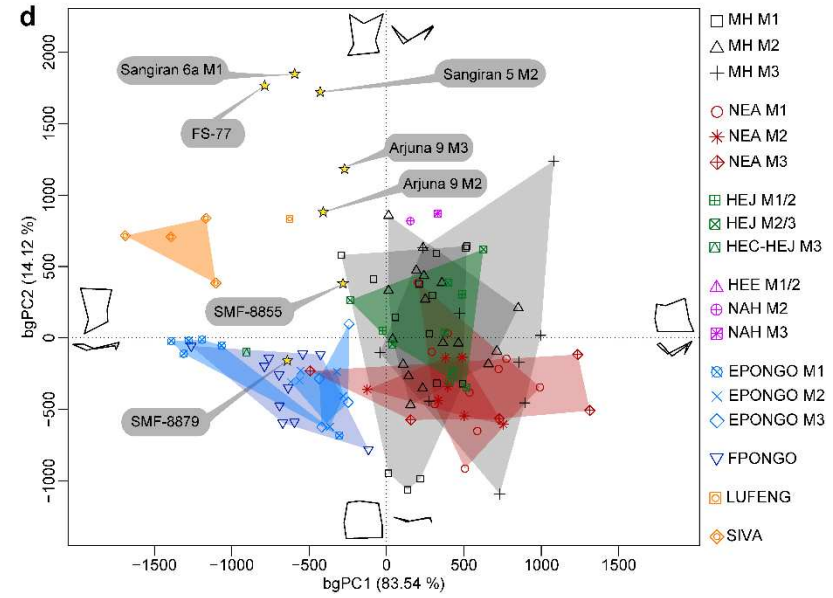
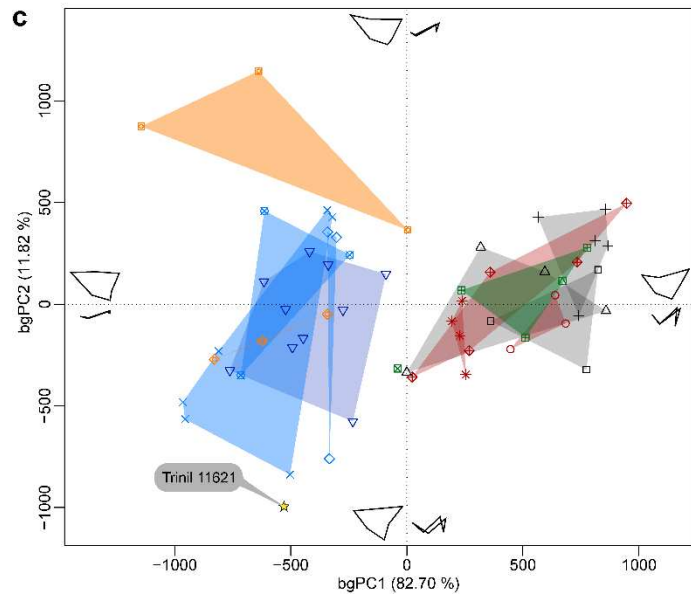
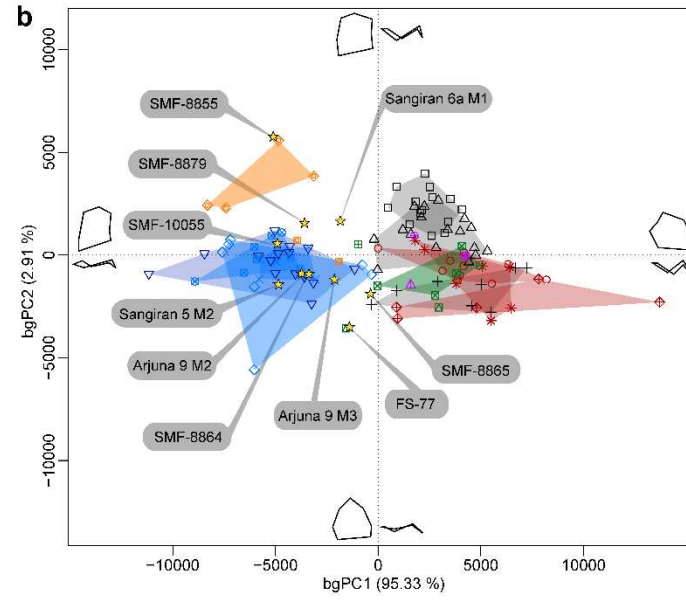
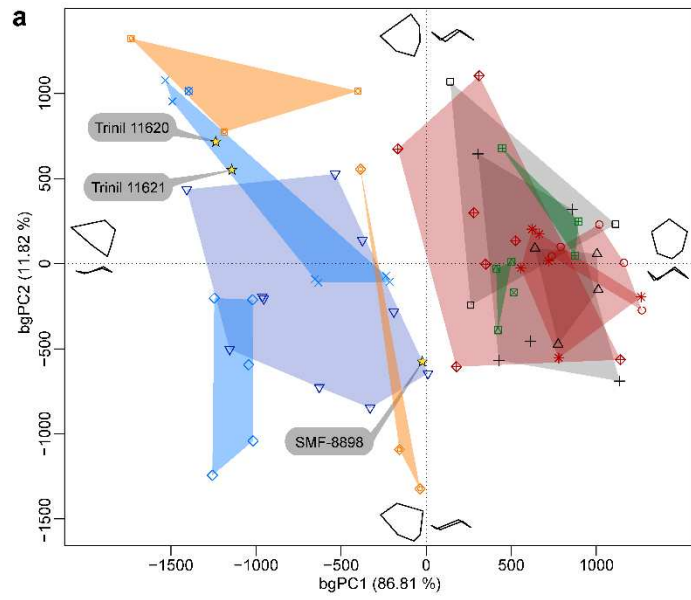
676
677

678 **Figure 3 | Enamel thickness cartographies.** **a**, Maxillary molars, **b**, Mandibular molars. The Indonesian hominid teeth (Supplementary Table 1)
679 are compared with fossil and extant hominid specimens. EPONGO, extant *Pongo*; FPONGO, fossil *Pongo*; HEJ, *H. erectus* from Java;
680 LUFENG, *Lufengpithecus*; MH, modern humans; NAH, North African late Early Pleistocene *Homo*; SIVA, *Sivapithecus* (Supplementary Table
681 2). Independently from Irrespective of their original side, all specimens are displayed as right anteriors in a slightly oblique occlusal perspective.
682 Scale bar, 10 mm.



683
684
685
686
687
688
689

Figure 4 | Molar crown-root proportions. **a, b**, The crown-root ratio (CRR, in %) and its adjusted Z-score statistics for the Indonesian hominid (IH) maxillary molars from Trinil compared with fossil and extant hominid specimens/samples. **c, d**, Similar comparative analyses for the mandibular molars of Sangiran 6a and Arjuna 9 (Supplementary Table 1). EPONGO, extant *Pongo*; HEC, *H. erectus* from China; HEJ, *H. erectus* from Java; LUFENG, *Lufengpithecus*; MH, modern humans; NAH; North African late Early *Homo*; NEA, Neanderthals; SIVA, *Sivapithecus* (Supplementary Table 2).



- MH M1
- △ MH M2
- + MH M3
- NEA M1
- * NEA M2
- ◇ NEA M3
- HEJ M1/2
- ▣ HEJ M2/3
- ▤ HEC-HEJ M3
- △ HEE M1/2
- ⊕ NAH M2
- ⊖ NAH M3
- ⊗ EPONGO M1
- ⊘ EPONGO M2
- ◇ EPONGO M3
- ▽ FPONGO
- LUFENG
- ◇ SIVA

691

692

693

694

695

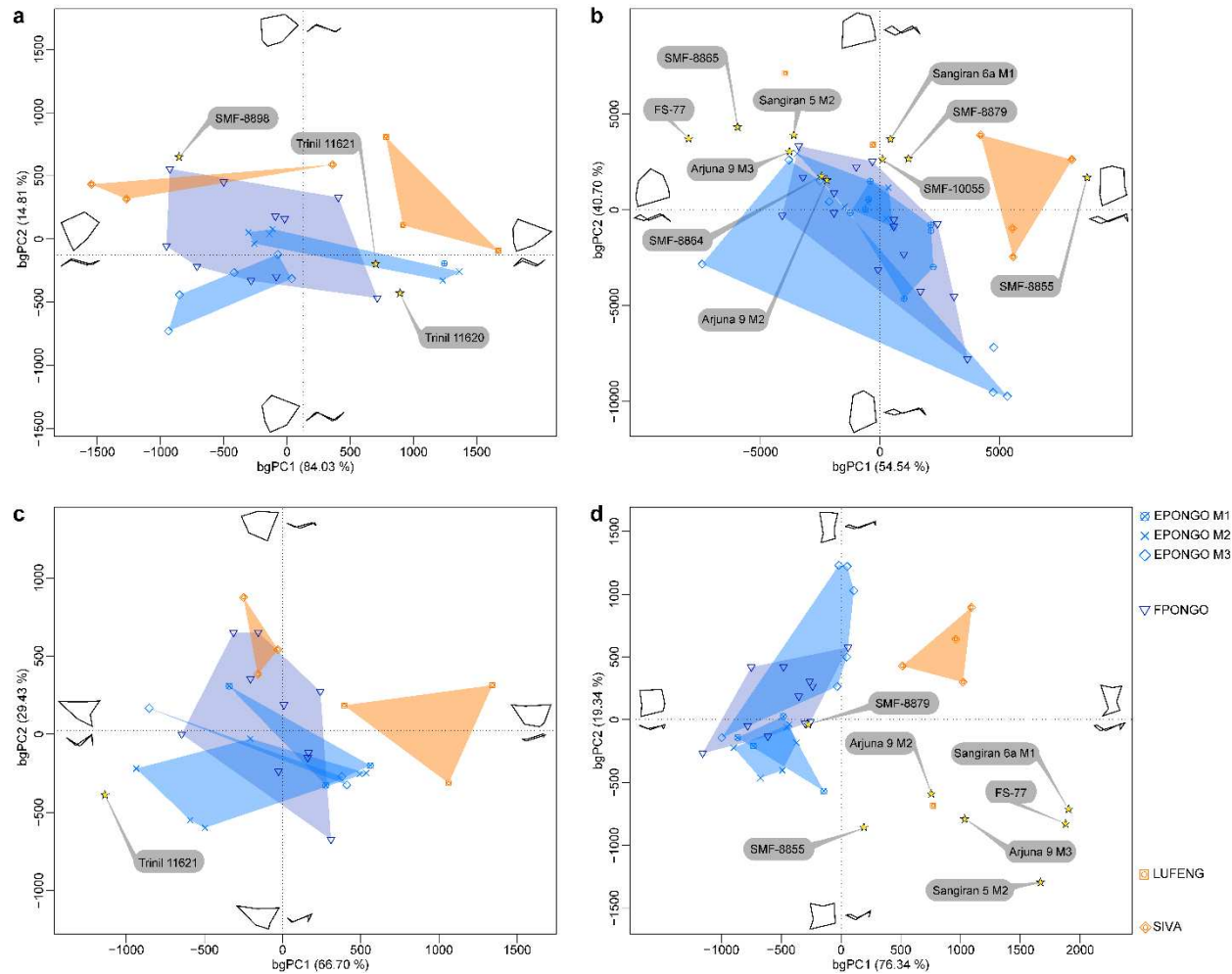
696

697

698

699

Figure 5 | Geometric morphometric analyses of the EDJ and pulp chamber. a, b, Between-group principal component analyses (bgPCA) of the 3D landmarks Procrustes-registered shape coordinates of the Indonesian hominid maxillary (**a**) and mandibular (**b**) molar EDJs (Supplementary Table 1) compared with fossil and extant hominid specimens/samples. **c, d,** bgPCA of the underlying maxillary (**c**) and mandibular (**d**) pulp cavity. The wireframes at the end of the axes illustrate the extreme morphological variation trends along each bgPC in occlusal (mesial aspect upward) and buccal views (mesial aspect rightward). EPONGO, extant *Pongo*; FPONGO, fossil *Pongo*; HEC, *H. erectus* from China; HEE, *H. erectus/ergaster* from Eritrea; HEJ, *H. erectus* from Java; LUFENG, *Lufengpithecus*; MH, modern humans; NAH, North African late Early Pleistocene *Homo*; NEA, Neanderthals; SIVA, *Sivapithecus* (Supplementary Table 2).



700
701
702
703
704
705
706

Figure 6 | Geometric morphometric analyses of the EDJ and pulp chamber in non-*Homo* hominids. **a, b,** Between-group principal component analyses (bgPCA) of the 3D landmarks Procrustes-registered shape coordinates of the Indonesian hominid maxillary (**a**) and mandibular (**b**) molar EDJs ([Supplementary Table 1](#)) compared with fossil and extant non-*Homo* hominid samples. **c, d,** bgPCA of the underlying maxillary (**c**) and mandibular (**d**) pulp cavity. The wireframes at the end of the axes illustrate the extreme morphological variation trends along each bgPC in occlusal (mesial aspect upward) and buccal views (mesial aspect rightward). EPONGO, extant *Pongo*; FPONGO, fossil *Pongo*;

707 LUFENG, *Lufengpithecus*; SIVA, *Sivapithecus* (Supplementary Table 2).